

Geometric Algorithm for Abelian-Gauge Models

V. Azcoiti, E. Follana and A. Vaquero

*Departamento de Física Teórica, Universidad de Zaragoza,
Cl. Pedro Cerbuna 12, E-50009 Zaragoza (Spain)
E-mail: azcoiti@azcoiti.unizar.es, efollana@unizar.es, alexv@unizar.es*

G. Di Carlo

*INFN, Laboratori Nazionali del Gran Sasso,
67010 Assergi, (L'Aquila) (Italy)
E-mail: gdicarlo@lngs.infn.it*

ABSTRACT:

Motivated by the sign problem in several systems, we have developed a geometric simulation algorithm based on the strong coupling expansion which can be applied to abelian pure gauge models. We have studied the algorithm in the $U(1)$ model in 3 and 4 dimensions, and seen that it is practical and is similarly efficient to the standard heat-bath algorithm, but without the ergodicity problems which comes from the presence of vortices. We have also applied the algorithm to the Ising gauge model at the critical point, and we find hints of a better asymptotic behaviour of the autocorrelation time, which therefore suggests the possibility of a smaller dynamical critical exponent with respect to the standard heat-bath algorithm.

Contents

1. Introduction	1
2. Abelian groups	3
3. Observables	4
4. Implementation and numerical results	6
5. The three dimensional Ising gauge model	12
6. Conclusions and Outlook	14

1. Introduction

The expected scenario for the phase diagram of QCD in the chemical potential–temperature plane is based on the conjecture that, besides the well established hadronic and quark-gluon plasma phases, there exists a new state of matter. This new phase is characteristic of the high density, low temperature regime: the asymptotic freedom of QCD and the known instability of large Fermi spheres, in the presence of weak attractive forces, results in a pairing of quarks with momenta near the Fermi surface (in analogy with the Cooper pairing in solid state systems at low temperature). A condensation of quark pairs should be the distinctive signal of the new phase and it has indeed been predicted using simplified phenomenological models of QCD. Unfortunately the lattice approach, the most powerful tool to perform first principles, non perturbative studies, is afflicted in the case of finite density QCD by the well known sign problem that, notwithstanding a large amount of work by many people [1], has prevented until now any significant step towards the understanding of this new phase.

An alternative strategy to overcome the sign problem consists in reformulating the theory, not in terms of the microscopic degrees of freedom (quarks and gluons in the QCD case), but in perhaps some other more physical variables (mesons, baryons, etc. [2, 3]). Following this line Karsch and Mütter [2] analyzed the phase diagram of strongly coupled QCD with SU(3) gauge fields, staggered fermions and four flavors. By integrating out the SU(3) gauge fields [4] Karsch and Mütter constructed a new representation of the QCD partition function as a statistical system of monomers, dimers and polymers (MDP-system). Even if at finite density some of the Boltzmann weights were still negative in the new QCD representation, they claimed that the dominant contributions to the partition function had positive weights; and this allowed for the construction of an algorithm that generates configurations distributed according to the absolute value of the integration measure, with the sign of the Boltzmann weights being absorbed into the observables.

Unfortunately the continuum limit of QCD lies not in the strong coupling regime but in the weak coupling regime, and here the pure gauge Boltzmann factor strongly changes the gauge integration rules [4], invalidating the MDP-QCD representation for the partition function. Indeed the MDP representation would be the zeroth order expansion of the partition function in powers of β , the square of the inverse gauge coupling.

The Karsch and Mütter results for the strong coupling limit of finite density QCD could, in principle, be extended to higher order in the expansion in β . This extension will obviously increase the complexity of the graphs contributing to the new representation of the QCD partition function, and furthermore, it is not clear at all whether the sign problem in the new representation will become a weak sign problem, as in the strong coupling case, or a severe sign problem [5]. In any case, the physical relevance of the system under consideration makes it worthwhile to try such a line of research. In addition there are other physically relevant gauge models with a sign problem, such as systems with a topological θ -term in the action, where these techniques could also be applied [6–15].

Several years ago Prokofev and Svistunov [16] proposed new algorithms for classical statistical spin systems, the worm algorithms, based on the use of a new representation of the partition function for these systems which emerges from the high temperature expansion. The use of this expansion involves introducing a new configuration space for the Ising model made up from monomers, dimers and closed paths, with their corresponding exclusion rules. Prokofev and Svistunov showed how these worm algorithms applied to several spin systems essentially eliminate critical slowing down, with dynamic critical exponents close to zero, and yet remain local. These results have been recently corroborated in [17] for the Ising model, reporting a detailed error analysis and a generalization of the method of [16].

Our aim in this paper is to construct and apply algorithms for the strong coupling representation of the partition function of three and four-dimensional abelian pure gauge models, in particular $U(1)$ and $Z(2)$ [18]. Independently of our aforementioned motivation, it seems interesting to us to construct these algorithms and to compare them with standard ones, such as heat-bath, in order to see if, as reported in [16, 17, 19] for spin systems, critical slowing down is also practically absent in gauge systems. This is precisely the reason why we have also simulated the three-dimensional Ising-gauge model. Indeed contrary to the $U(1)$ model, the three-dimensional Ising-gauge model, which is dual of the Ising model in three dimensions, shows a second order phase transition where critical slowing down is present in the standard algorithms. The generalization of the strong coupling representation of the partition function to the $U(1)$ model with dynamical fermion matter fields, which in principle suffers from the sign problem [20], will be reported in a forthcoming publication.

The paper is organized as follows. In section II we analyze the strong coupling representation of the partition function, discuss the possible structures which can appear in the abelian model, and compute the configuration transition probabilities for local changes. Section III shows how to compute in the new representation thermodynamic quantities, such as the plaquette energy, specific heat, Wilson loops and correlation functions. In section IV we describe the implementation of our algorithm, report numerical results for the three and four dimensional $U(1)$ compact model, and compare the efficiency of our algorithm against heat-bath. Section V contains our results for the three-dimensional Ising-gauge model which, as stated before, is a good laboratory to check the

efficiency of the algorithm near second order phase transition points. Last section is devoted to summarize our conclusions and discuss possible extensions of this work.

2. Abelian groups

We will consider an (euclidean) abelian $U(1)$ gauge theory on the lattice with the usual Wilson action,

$$S = -\beta \text{Re} \sum_{\substack{n, \mu, \nu \\ \mu < \nu}} U_\mu(n) U_\nu(n + \mu) U_\mu^\dagger(n + \nu) U_\nu^\dagger(n) = - \sum_{k=1}^{N_p} \frac{\beta}{2} (U_k + U_k^*) \quad (2.1)$$

where N_p is the number of plaquettes of the lattice, k indexes the plaquettes of the lattice and U_k and U_k^* are the oriented product of gauge fields along plaquette k and its complex conjugate respectively.

The starting point of the algorithm is the strong-coupling expansion of the partition function:

$$\begin{aligned} \mathcal{Z} &= \int [\prod_{n, \mu} dU_\mu(n)] \prod_{k=1}^{N_p} e^{\frac{\beta}{2}(U_k + U_k^*)} = \int [\mathcal{D}U] \prod_k \left\{ \sum_{n=0}^{\infty} \frac{(\frac{\beta}{2})^n}{n!} (U_k + U_k^*)^n \right\} = \\ &= \int [\mathcal{D}U] \prod_k \left\{ \sum_{n=0}^{\infty} \frac{(\frac{\beta}{2})^n}{n!} \left[\sum_{j=0}^n \binom{n}{j} (U_k)^j (U_k^*)^{n-j} \right] \right\} = \\ &= \int [\mathcal{D}U] \prod_k \left\{ \sum_{j_1, j_2=0}^{\infty} \frac{(\frac{\beta}{2})^{j_1+j_2}}{(j_1+j_2)!} \binom{j_1+j_2}{j_1} (U_k)^{j_1} (U_k^*)^{j_2} \right\} \quad (2.2) \end{aligned}$$

If we expand the product over the plaquettes we get a sum of terms, which can be uniquely labeled by giving a couple of natural numbers for each plaquette $(n_k^\alpha, \bar{n}_k^\alpha)$, where n_k^α and \bar{n}_k^α correspond to the powers of U_p and U_p^* and the super-index α refers to a specific term in the expansion. After integration over the gauge fields, the only non-vanishing contributions to \mathcal{Z} are those in which every link corresponding to a plaquette with $(n_k^\alpha, \bar{n}_k^\alpha) \neq (0, 0)$ appears accompanied by its complex conjugate. Each of these contributions therefore can consist only of plaquettes with $n_k^\alpha = \bar{n}_k^\alpha$, and plaquettes which form closed orientable surfaces. We can write

$$\mathcal{Z}(\beta) = \sum_{\alpha} C^\alpha(\beta) \quad (2.3)$$

where α indexes the set of non-vanishing contributions. The (non-negative) weight corresponding to such a contribution is given by

$$C^\alpha(\beta) = \prod_k \frac{\beta^{n_k^\alpha + \bar{n}_k^\alpha}}{2^{n_k^\alpha + \bar{n}_k^\alpha} n_k^\alpha! \bar{n}_k^\alpha!} \quad (2.4)$$

Now we can view \mathcal{Z} as the partition function of a new system, where a configuration α is characterized by the set of numbers $(n_k^\alpha, \bar{n}_k^\alpha)$ corresponding to a non-vanishing contribution to the strong coupling expansion, with probability $w^\alpha = C^\alpha/\mathcal{Z}$, and implement a Monte Carlo in this new configuration space. We define elementary Monte Carlo moves consisting in adding a “double plaquette”, $(n_k^\alpha, \bar{n}_k^\alpha) \rightarrow (n_k^\alpha + 1, \bar{n}_k^\alpha + 1)$ (as well as the opposite move, if both $n_k^\alpha, \bar{n}_k^\alpha > 0$), and adding an

elementary cube (as well as removing it if present). This ensures that we stay inside the set of non-vanishing contributions. We choose the transition probabilities to be proportional to the weights of the corresponding configurations in the partition function, which ensures detailed balance. This can be done efficiently, and it is also easy to see that the algorithm is ergodic.¹

The gauge Z_p model can be handled in the same way, the only difference being that now there are additional non-vanishing contributions given by powers of p of the plaquette or its complex conjugate, that is, we must allow contributions with $n_k^\alpha - \bar{n}_k^\alpha = 0 \pmod{p}$. The weight of a configuration is given by the same expression as before (2.4). The only modification required in the algorithm is adding a new move which creates or destroys a p power of the plaquette or its complex conjugate.

3. Observables

The computation of observables is quite easy in this representation. The definition of the observable plaquette² is

$$\langle P_\square \rangle = \frac{1}{N_P} \partial_\beta \ln(Z) \quad (3.1)$$

Using (2.3) and (2.4), we obtain

$$\langle P_\square \rangle = \frac{1}{N_P} \partial_\beta \ln \left(\sum_{\alpha \in \mathcal{C}} C^\alpha \right) = \frac{1}{N_P} \frac{1}{Z} \sum_{\alpha \in \mathcal{C}} \frac{(n^\alpha + \bar{n}^\alpha)}{\beta} C^\alpha \quad (3.2)$$

with

$$n^\alpha = \sum_{k=1}^{N_P} n_k^\alpha$$

$$\bar{n}^\alpha = \sum_{k=1}^{N_P} \bar{n}_k^\alpha$$

The quantity C^α/Z is the probability w^α of each configuration α . The mean of the observable plaquette is then

$$\langle P_\square \rangle = \frac{1}{\beta N_P} \sum_{\alpha \in \mathcal{C}} w^\alpha (n^\alpha + \bar{n}^\alpha) \quad (3.3)$$

that is to say, the observable plaquette is equal to the mean value of the sum of the occupation numbers n^α plus \bar{n}^α divided by β and normalized by N_P .

Another interesting observable is the specific heat

$$C_V = \partial_\beta \langle P_\square \rangle \quad (3.4)$$

¹A single surface that wraps around the lattice cannot be created by this algorithm starting from the empty configuration, but this is only a finite-volume correction.

²We must remark that the observable plaquette and the plaquettes living in our lattice are not the same, although they are strongly related. The observable plaquette refers to the minimal Wilson loop, whereas the plaquettes refers to geometric entities, living on the lattice. In order to keep the discussion clear, we will always refer to the minimal Wilson loop as *observable plaquette*.

We can profit from the previous expression of P_\square (3.3) to find the following equation

$$C_V = \frac{1}{N_P} \left\{ \sum_{\alpha \in C} w^\alpha \frac{(n^\alpha + \bar{n}^\alpha)^2}{\beta^2} - \left(\sum_{\alpha \in C} w^\alpha \frac{(n^\alpha + \bar{n}^\alpha)}{\beta} \right)^2 - \sum_{\alpha \in C} w^\alpha \frac{(n^\alpha + \bar{n}^\alpha)}{\beta^2} \right\} \quad (3.5)$$

Sometimes, it is interesting to compute correlation observables, such as the Wilson loop (larger than the single observable plaquette), or the plaquette–plaquette correlation function. To compute these it will prove helpful to introduce a couple of variable coupling constants $\{\beta_k, \bar{\beta}_k\}$, which depend on the plaquette site k , in such a way that the partition function reads now

$$\mathcal{Z}(\beta_j, \bar{\beta}_j) = \int [dU] \prod_k e^{\left(\frac{\beta_k}{2} U_k + \frac{\bar{\beta}_k}{2} U_k^*\right)} \quad (3.6)$$

The weight of the configurations changes accordingly

$$C^\alpha(\beta_j, \bar{\beta}_j) = \prod_{k=1}^{N_P} \frac{\beta_k^{n_k^\alpha} \bar{\beta}_k^{\bar{n}_k^\alpha}}{2^{n_k^\alpha + \bar{n}_k^\alpha} (n_k^\alpha!) (\bar{n}_k^\alpha!)} \quad (3.7)$$

Now the correlation functions or the Wilson loops are computed by simple derivation, and then taking all the $\beta_k, \bar{\beta}_k$ to the same value. For instance, the 2×1 Wilson loop can be calculated as

$$\langle P_{W_{2 \times 1}} \rangle = 2^2 \lim_{\beta_j, \bar{\beta}_j \rightarrow \beta} \frac{\sum_{\alpha \in C} \partial_{\beta_k} \partial_{\bar{\beta}_{k+1}} C^\alpha(\beta_j, \bar{\beta}_j)}{\sum_{\alpha \in C} C^\alpha(\beta_j, \bar{\beta}_j)} = 2^2 \sum_{\alpha \in C} \frac{n_k^\alpha \bar{n}_{k+1}^\alpha}{\beta^2} w^\alpha \quad (3.8)$$

where k and $k+1$ are contiguous plaquette sites. The generalization of this result to larger planar Wilson loops is straightforward. Indeed the expectation value of any planar Wilson loop can be computed as the mean value of the product, for all plaquettes enclosed by the loop, of the occupation number of plaquettes in each plaquette site, multiplied by a factor $2/\beta$ to a power which is just the number of plaquettes enclosed by the loop. This observable is quite remarkable, for it is computed as a product of occupation numbers, and features a $(2/\beta)^{Area}$ factor, which eventually may become exponentially large or small, as the size of the loop increases. All these particular facts render this observable hard to compute, as we will see in the numerical results.

In the same way we can also obtain the correlation functions for two arbitrary plaquettes of the lattice:

$$\langle U_k U_l \rangle = 2^2 \lim_{\beta_j, \bar{\beta}_j \rightarrow \beta} \frac{\sum_{\alpha \in C} \partial_{\beta_k} \partial_{\bar{\beta}_l} C^\alpha(\beta_j, \bar{\beta}_j)}{\sum_{\alpha \in C} C^\alpha(\beta_j, \bar{\beta}_j)} = 2^2 \sum_{\alpha \in C} \frac{n_k^\alpha \bar{n}_l^\alpha}{\beta^2} w^\alpha \quad (3.9)$$

and

$$\langle U_k U_l^* \rangle = 2^2 \lim_{\beta_j, \bar{\beta}_j \rightarrow \beta} \frac{\sum_{\alpha \in C} \partial_{\beta_k} \partial_{\bar{\beta}_l} C^\alpha(\beta_j, \bar{\beta}_j)}{\sum_{\alpha \in C} C^\alpha(\beta_j, \bar{\beta}_j)} = 2^2 \sum_{\alpha \in C} \frac{n_k^\alpha \bar{n}_l^\alpha}{\beta^2} w^\alpha \quad (3.10)$$

Finally from (3.9) and (3.10) and taking into account the symmetry of the model we can write:

$$\langle \text{Re} U_k \text{Re} U_l \rangle_c = \frac{1}{\beta^2} \langle (n_k + \bar{n}_k) (n_l + \bar{n}_l) \rangle - \langle n_k + \bar{n}_k \rangle \langle n_l + \bar{n}_l \rangle \quad (3.11)$$

$$\langle \text{Im} U_k \text{Im} U_l \rangle_c = -\frac{1}{\beta^2} \langle (n_k - \bar{n}_k) (n_l - \bar{n}_l) \rangle \quad (3.12)$$

where the brackets denote average over configurations.

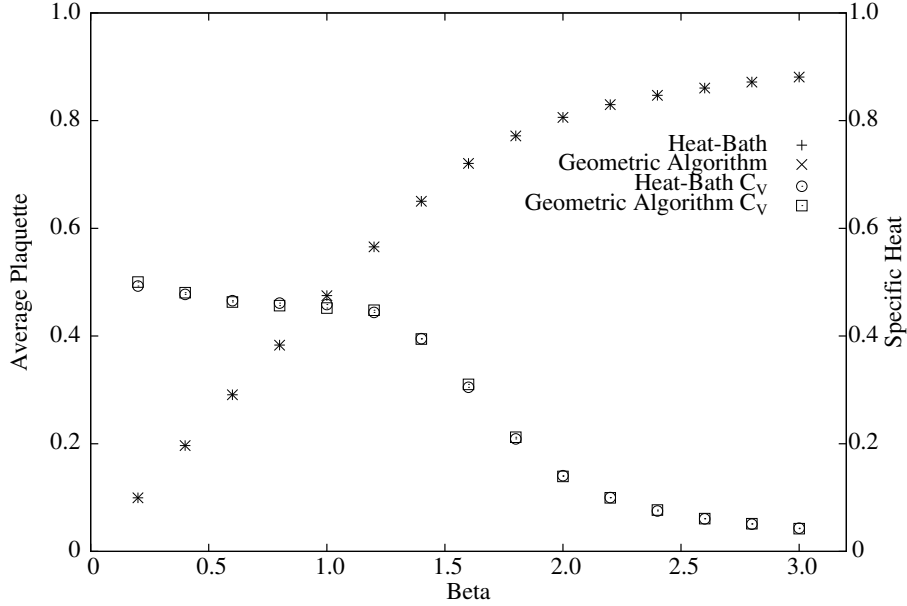


Figure 1: Three dimensional U(1) lattice gauge system. Errors are smaller than symbols.

4. Implementation and numerical results

In order to see our algorithm (which we should call, from now on, *geometric algorithm*) at work, we have performed numerical simulations of several lattice gauge theory systems, in three and four dimensions. Our aim is to check the goodness of our approach, comparing the results we obtain using the geometric algorithm with those obtained from more standard ones; hence we want to compare the properties of the algorithm itself, in term of numerical efficiency and autocorrelation times with, for example, the usual heat-bath algorithm. We have in mind the results of [17] where it was claimed that with a similar algorithm, at a second order critical point in a non-gauge system, there is a very strong reduction in the critical slowing down.

Let us start with the three dimensional U(1) lattice gauge model: this model is known to have a single phase from strong to weak coupling. We have chosen to measure two simple observables, namely the plaquette observable and the specific heat, following the definitions given in the preceeding Section. We have simulated the model with our algorithm and with a standard heat-bath for a large interval of β values using a 12^3 lattice; we allowed the system to reach thermalization for 5×10^4 iterations and then measured the observables for 10^6 iterations. Errors are evaluated using a Jackknife procedure. The results are shown in Fig 1. We can easily see in this figure that the two simulations give essentially the same results.

Almost the same situation can be depicted also for the four dimensional U(1) model; the results of a similar set of simulations, performed with the two algorithms on a 16^4 lattice, are shown in Fig 2. Here the only difference can be seen near the phase transition point. Remember that due to the difference in finite volume terms between the two algorithms, the precise pseudo-critical coupling value at finite volume has to be slightly different.

These results allow us to infer that the geometric approach is able to reproduce all the features of the models under investigation, and when differences are seen they can be easily explained on

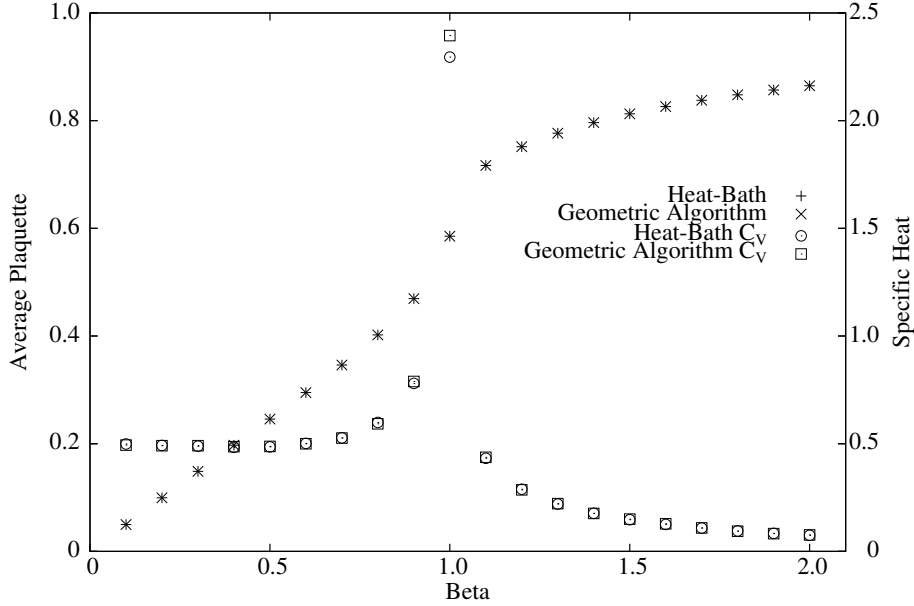


Figure 2: Four dimensional U(1) lattice gauge system; please note the different scale for the specific heat on the right. Largest errors (those on the pseudo-critical point) are smaller than symbols.

the difference between finite volume terms.

The presence of two clearly different phases in this model, namely a confining and a Coulomb one, allows us to study the behaviour of the Wilson loop results in two different physical situations; as above we have also performed standard simulations for a cross check between the two approaches. In Figs. 3 and 4 we report the behaviour of the Wilson loop in both phases (confining in Fig. 3 and Coulomb in Fig. 4) and in lattices of different size (12^4 , 14^4 , 16^4).

These figures deserve some comments. The geometric algorithm seems to suffer from larger statistical errors than the heat-bath method, regardless of the phase of the system. To understand this result, we should have a close look at the inner machinery of the algorithm, in particular, the way the Wilson loop is computed (see eq. (3.8)). First of all, the mean value of the Wilson loop is computed as a sum of integer products, implying the existence of large fluctuations between configurations. For example, doubling the occupation number of a single plaquette doubles the value of the loop. This is a quite common fluctuation at the β values of our simulations, and the fluctuations will increase as the loop (and therefore the number of plaquettes) grows. To complicate the computation further, we are trying to calculate an exponentially small quantity by summing integer numbers. The discrete nature of this computation tells us that non-zero values of the quantity must appear with an exponentially small probability. This explains the inherent difficulties of the large Wilson loops (4×4 and greater) measurement in the confining phase. The result is shown in Fig. 3: the mean value of the 5×5 Wilson loop was exactly zero in the geometric algorithm, which is of course wrong. Finally, the expectation value of the Wilson loop is proportional to a $(2/\beta)^A$ factor, A being the loop area. This value may become huge (or tiny) for large loops and low (or high) values of beta, thus enhancing the problems that arise from the discreteness of the algorithm.

Notwithstanding the larger fluctuations in the large Wilson loops within the geometric algorithm discussed above, our algorithm has a clear advantage against heat-bath: it does not suffer

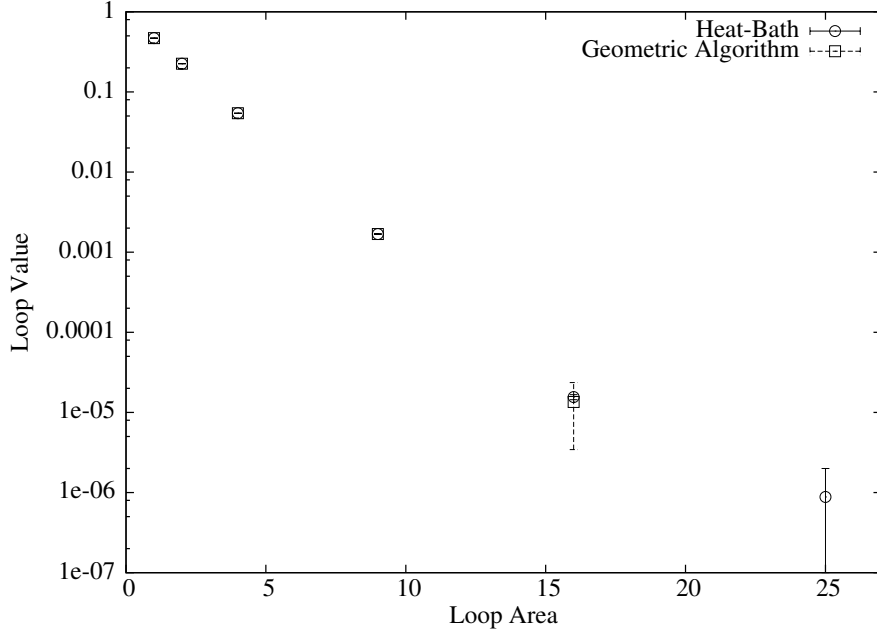


Figure 3: Real part of the Wilson loop versus the loop area for the confining phase ($\beta = 0.9$) in the four-dimensional U(1) gauge model. Notice the absence of the 5×5 loop in the geometric algorithm. The lattice volume was 16^4 .

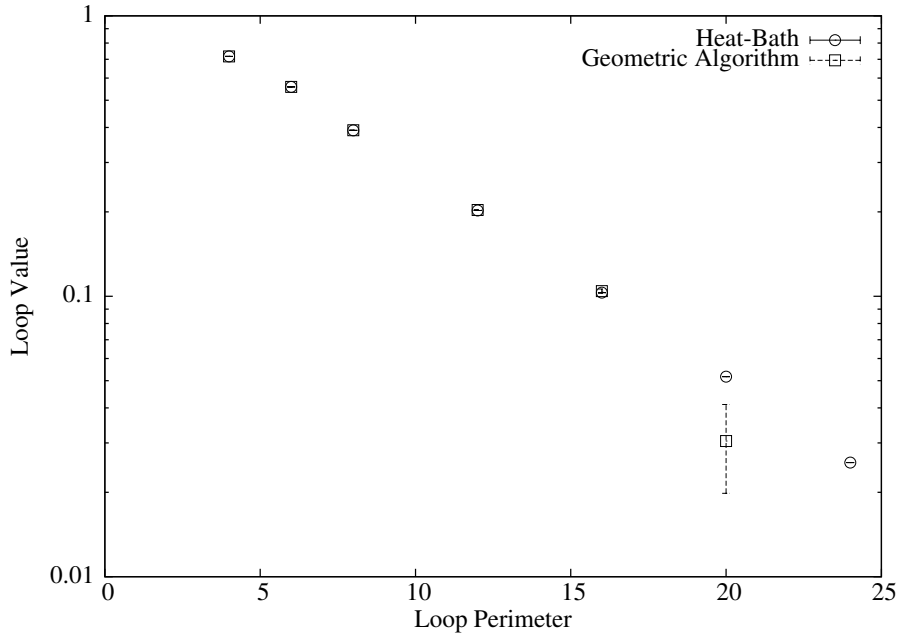


Figure 4: Real part of Wilson loop versus the loop perimeter for the Coulomb phase ($\beta = 1.1$) in the four-dimensional U(1) gauge model. The lattice volume was 16^4 .

from ergodicity problems. Indeed the results for the Wilson loop at $\beta = 3$ reported in Fig. 5 strongly support the previous statement. The points obtained with the geometric algorithm nicely follow the weak coupling prediction of [21], whereas the heat-bath results for large Wilson loops,

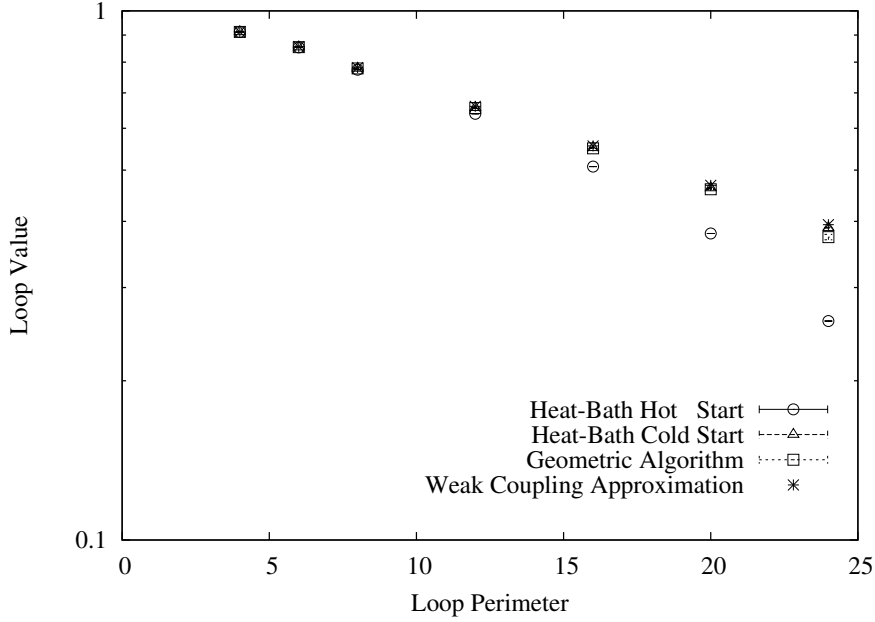


Figure 5: Real part of Wilson loop versus the loop perimeter for a large β value ($\beta = 3.0$) in the four-dimensional U(1) gauge model. Notice the difference of performance between the hot and the cold starts of the Heat-Bath algorithm. The lattice volume was 12^4 .

obtained from a hot start, clearly deviate from the analytical weak coupling prediction. The origin of this anomalous behavior in the heat-bath case is related to the formation of vortices, which are metastable states, that become extremely long lived in the Coulomb phase [22].

We have also calculated the plaquette–plaquette correlation (of the real (3.11) and of the imaginary (3.12) parts) in both phases and for plaquettes living in the same plane. Here we expect a much milder behaviour for the geometrical algorithm, for there is no large $(2/\beta)^A$ factor, and the fluctuations are reduced to a couple of plaquettes. The results are shown in Figs. 6, 7, 8 and 9.

In all the cases the numerical results obtained with the geometric and heat-bath algorithms essentially agree, except for the correlations of the imaginary part of the plaquettes in the Coulomb phase (Fig. 9), where a clear discrepancy for distances larger or equal than 4 is observed. Again in this case the reason for this discrepancy is related, as for the Wilson loop results previously discussed, to the formation of extremely long-lived metastable states [22] in the heat-bath simulations, which seem to be absent in the geometric algorithm. Indeed we have verified, with simulations in 12^4 lattices, that the discrepancies in the correlations of the imaginary part of the plaquettes in Coulomb phase at large distances basically disappear, when we start the heat-bath runs from a cold configuration. There are still small discrepancies in this case, but they can be reasonably attributed to the difference in finite volume terms between the two algorithms.

To compare computational costs we define a figure of merit which is the product of the squared error times the cpu time. We expect the error to vanish like $1/\sqrt{N_{\text{Monte Carlo}}}$, and therefore the quantity defined above should tend asymptotically to a constant. We show the value of this quantity for several observables in both phases and for both algorithms in Fig. 10. We can see that the performance of both algorithms is quite comparable. The differences that are seen could conceivably

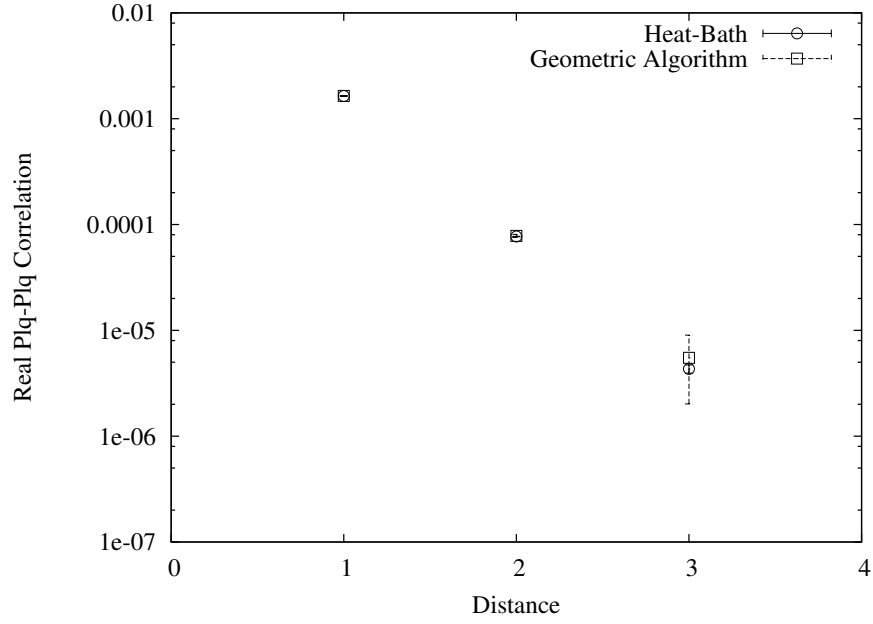


Figure 6: Correlation function of the plaquette real part versus plaquette–plaquette distance in lattice units, for the four-dimensional U(1) lattice gauge model in the confining phase ($\beta = 0.9$). Beyond distance 4, the error became far larger than the expectation value of the correlation. The lattice volume was 16^4 .

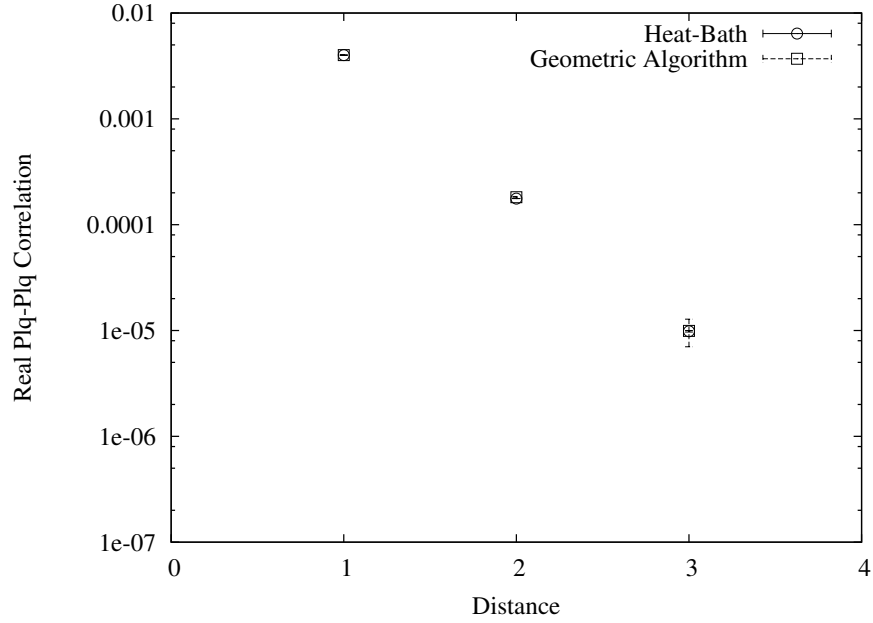


Figure 7: Correlation function of the plaquette real part versus plaquette–plaquette distance in lattice units, for the four-dimensional U(1) lattice gauge model in the Coulomb phase ($\beta = 1.1$). Beyond distance 4, the error became far larger than the expectation value of the correlation. The lattice volume was 16^4 .

change if one were to optimize the specific implementations, but none is obviously much more efficient than the other for the models studied.

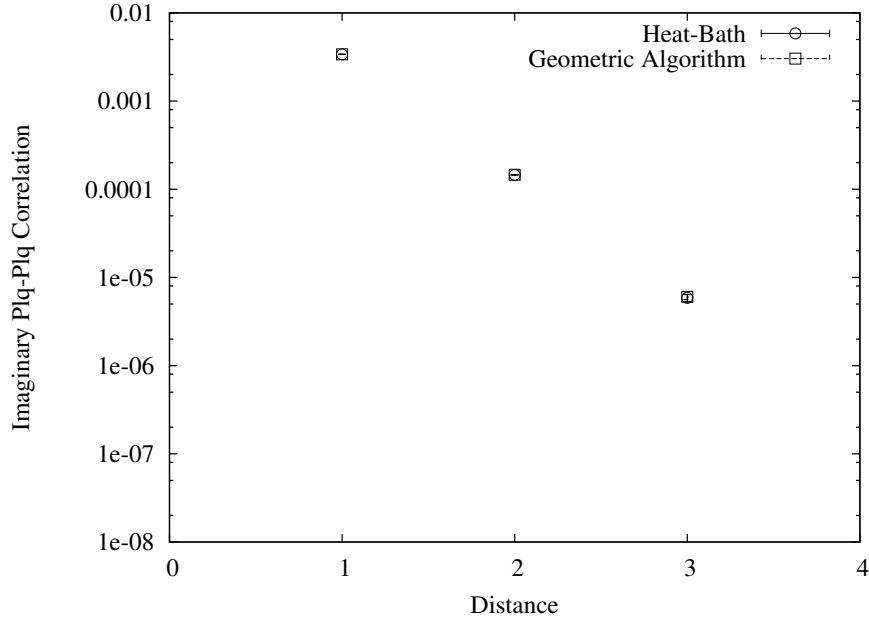


Figure 8: Correlation function of the plaquette imaginary part versus plaquette–plaquette distance in lattice units, for the four-dimensional U(1) lattice gauge model in the confining phase ($\beta = 0.9$). Beyond distance 4, the error became far larger than the expectation value of the correlation. The lattice volume was 16^4 .

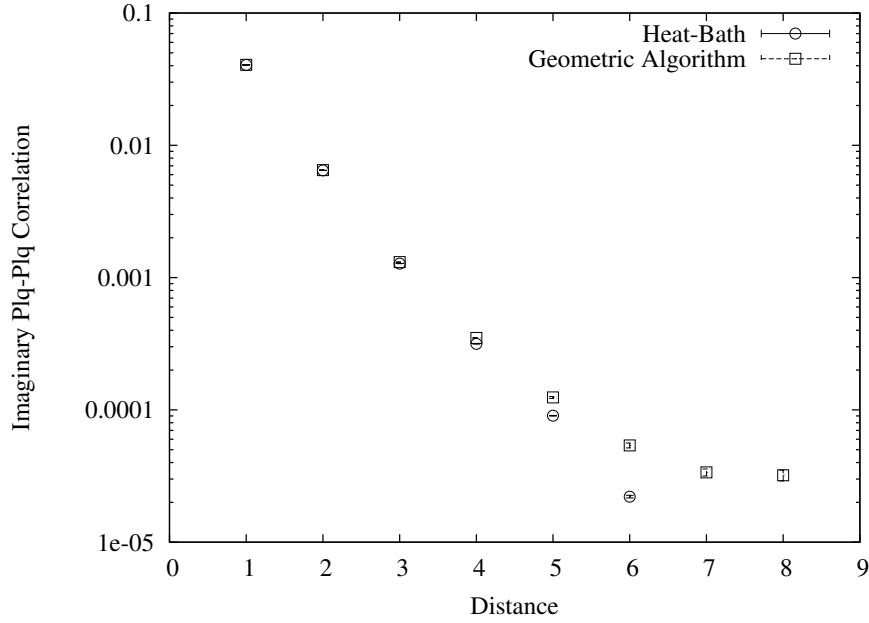


Figure 9: Correlation function of the plaquette imaginary part versus plaquette–plaquette distance in lattice units, for the four-dimensional U(1) lattice gauge model in the Coulomb phase ($\beta = 1.1$). Notice the different behaviour of the algorithms at large distances. The lattice volume was 16^4 .

In particular, for the plaquette observable and the specific heat, both algorithms have a similar figure of merit. From our point of view, the differences are not quite significant, and could change

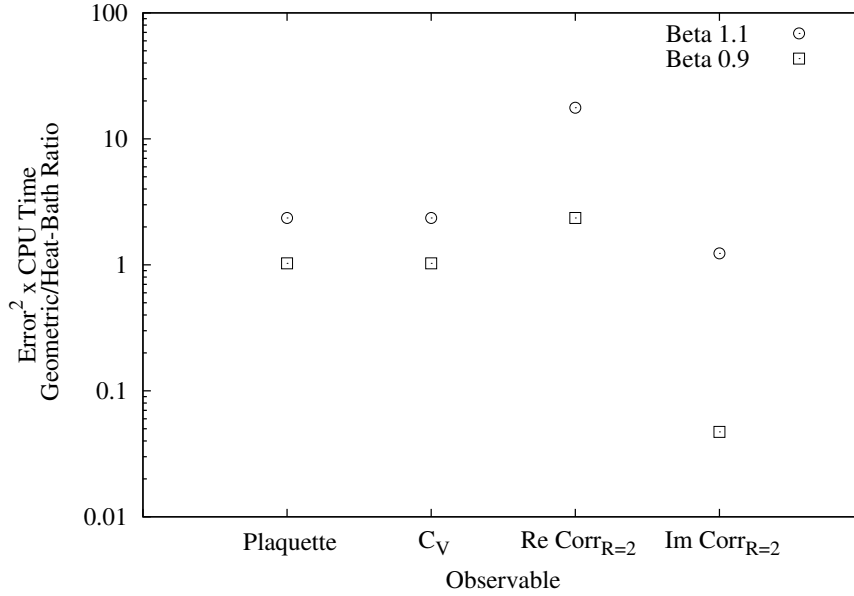


Figure 10: Ratios of figures of merit for different observables between geometric and heat-bath algorithms. Re Corr_R = 2 and Im Corr_R = 2 stand for Real and Imaginary plaquette–plaquette correlations at distance 2.

with careful optimizations. The real plaquette-plaquette correlation is quite another story, for the differences become significative in the Coulomb phase (a factor ≈ 20), but they do not become worse as β increases, as we test in a 12^4 simulation at $\beta = 3.0$.

On the other hand, the geometric algorithm seems to perform much better for the imaginary plaquette-plaquette correlation in the confining phase, whereas in the Coulomb phase all the advantage vanishes. Again, our 12^4 computation at $\beta = 3.0$ reveal that the ratio slowly decreases as β increases (being ≈ 0.8 at $\beta = 3.0$).

Of course, this analysis assumes that both algorithms have no ergodicity problems. We must be careful to start from a cold configuration when running the heat-bath simulations in the Coulomb phase, in order to avoid metastable states which could spoil the reliability of the simulation.

5. The three dimensional Ising gauge model

Let us finally come to the point of critical slowing down: this is a major issue as any improvement in this field can be of paramount importance in term of the cost of large scale simulations of (statistical) systems at a critical point. Beating critical slowing down is one of the main motivations in the development of new Monte Carlo algorithms.

Typically what is found in Monte Carlo simulations of system both in statistical physics and gauge theories is that the autocorrelation time τ diverges as we approach a critical point, usually as a power of the spatial correlation length: $\tau \sim \xi^z$, where ξ is the correlation length and z is a dynamical critical exponent. Usual local algorithms have values of z around 2, making it very inefficient to simulate close to the critical point. For spin systems there are well known cluster algorithms with much smaller z . Previously published results [17] on an algorithm similar to ours,

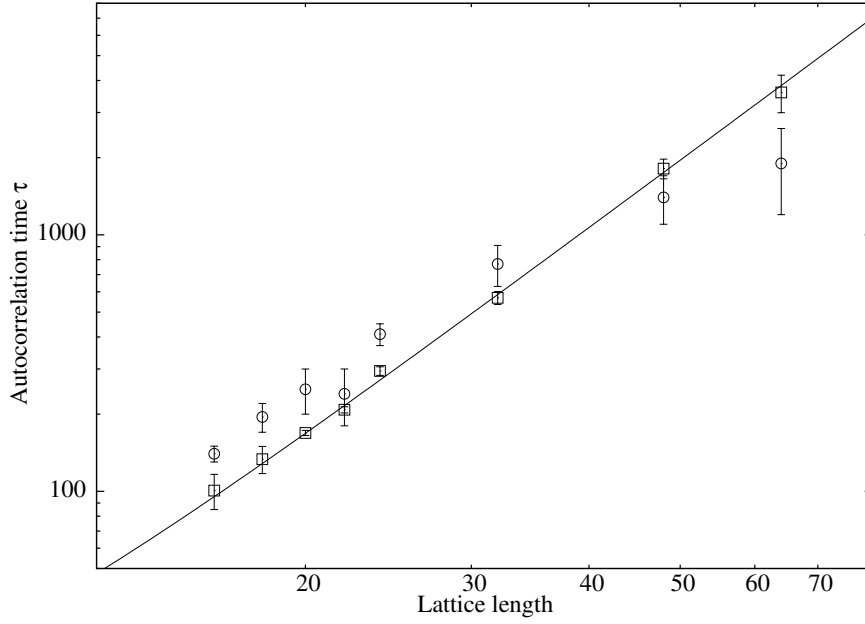


Figure 11: Autocorrelation times at the critical point versus lattice length; boxes stand for standard algorithm results, with a linear fit to guide the eye, while circles represent the results of the geometric algorithm. The errors were obtained by a jack-knife procedure.

but applied to a non-gauge model, have claimed a similarly smaller value for z . Having also this motivation in mind, we have investigated the autocorrelation properties of our numerical scheme on the critical point of a system that undergoes a second order phase transition (with diverging correlation length). Our model of choice has been the three dimensional Ising-gauge model. We have performed extensive simulations in the critical zone of this model for several values of the lattice size (and hence correlation length) using both the geometric algorithm and the standard Monte Carlo approach, the latter known to have a lower bound for the autocorrelation exponent z equal to 2, a value typical of all local algorithms.

For an observable O we define the autocorrelation function $\rho(t)$ as

$$\rho(t) = \frac{\langle (O(i) - O_A)(O(i+t) - O_B) \rangle}{\sqrt{\sigma_A^2 \sigma_B^2}} \quad (5.1)$$

where $O_A = \langle O(i) \rangle$, $O_B = \langle O(i+t) \rangle$, $\sigma_A^2 = \langle (O(i) - O_A)^2 \rangle$, $\sigma_B^2 = \langle (O(i+t) - O_B)^2 \rangle$, and $\langle \rangle$ denotes average over i . We then define the integrated autocorrelation time by

$$\tau = \rho(0) + 2 \sum_{t=1}^N \rho(t) \frac{N-t}{N} \quad (5.2)$$

where N is fixed but with $N < 3\tau$ and $N < 10\%$ of the total sample. In Fig. 11 we report the results for the integrated autocorrelation time of the plaquette versus lattice size in logarithmic scale for both algorithms. The results of our simulations hint to a different asymptotic behaviour of the autocorrelation time, although with our present data we cannot obtain a conclusive result. The

results for the heat-bath algorithm seem to fall nicely on a straight line, which would correspond to a simple exponential dependence of τ on L , with $z = 2.67 \pm 0.08$, but the geometric algorithm presents a more complicated behaviour, as well as larger errors. There are clear signs that the asymptotic behaviour should be better than the heat-bath, but much more extensive simulations, outside the scope of this work, would be needed to get a definite value for z .

6. Conclusions and Outlook

Our main motivation is the sign problem, particularly in QCD at finite chemical potential, but which appears also in other systems of interest, for example when a θ vacuum term is present. New ideas are clearly needed in order to make significant advances in this problem, and one possibility is the development of new simulation algorithms that might circumvent the difficulties of conventional approaches.

We have developed a geometric algorithm, based on the strong coupling expansion of the partition function, which can be applied to abelian pure gauge models. We have checked in the $U(1)$ model in 3 and 4 dimensions that the algorithm can be implemented efficiently, and is comparable with a standard heat-bath algorithm for those models. It seems however that the geometric algorithm does not suffer lack of ergodicity due to the presence of vortices, as can be the case with heat-bath, depending on the starting point.

We have also studied the algorithm in the 3 dimensional Ising gauge model at the critical point, where we have seen hints that the asymptotic behaviour of the geometric algorithm may be better than standard heat-bath. This would be very interesting, because in contrast to spin systems, where there exists cluster algorithms that can greatly reduce critical slowing-down, to our knowledge no similar algorithm is known for gauge systems. Our results are however not enough to establish this, and much more extensive simulations should be done to clarify this point.

The algorithm can be extended to include fermions, and this constitutes work in progress. In this case there is a sign problem, and one question we want to answer is whether such problem is severe or mild.

Acknowledgments

This work has been partially supported by an INFN-MEC collaboration, CICYT (grant FPA2006-02315) and DGIID-DGA (grant2007-E24/2). E. Follana is supported by Ministerio the Ciencia e Innovación through the Ramón y Cajal program.

References

- [1] *See, for instance*, M. P. Lombardo, *J. Phys. G* **35** 104019, (2008).
- [2] F. Karsch and K.H. Mütter, *Nucl. Phys. B* **313**, 541 (1989).
- [3] F. Palumbo, *Phys. Rev. D* **60** 074009, (1999).
- [4] P. Rossi and U. Wolff, *Nucl. Phys. B* **248**, 105 (1984).

- [5] J. W. Cherrington, *arXiv:0810.0546* [hep-lat] (2008).
- [6] W. Bietenholz, A. Pochinsky, U.J. Wiese, *Phys. Rev. Lett.* **75**, 4524-4527, (1995).
- [7] V. Azcoiti, G. Di Carlo, A. Galante, V. Laliena, *Phys. Rev. Lett.* **89**, 141601, (2002).
- [8] J. Ambjorn, K. N. Anagnostopoulos, J. Nishimura, J.J.M. Verbaarschot, *JHEP*, 0210:062, (2002).
- [9] M. D'Elia, *Nucl. Phys. B* **661**, 139, (2003).
- [10] V. Azcoiti, G. Di Carlo, A. Galante, V. Laliena, *Phys. Rev. D.* **69**, 056006, (2004).
- [11] M. Imachi, Y. Shinno, H. Yoneyama, *Prog. Theor. Phys.* **111**, 387, (2004).
- [12] L. Del Debbio, G.M. Manca, H. Panagopoulos, A. Skouroupathis, E. Vicari, *JHEP*, 0606:005, (2006).
- [13] V. Azcoiti, G. Di Carlo, A. Galante, *Phys. Rev. Lett.* **98**, 257203, (2007).
- [14] B. Alles, A. Papa, *Phys. Rev. D* **77**, 056008, (2008).
- [15] E. Vicari, H. Panagopoulos, *Phys. Rept.* **470**, 93, (2009).
- [16] N. Prokofev and B. Svistunov, *Phys. Rev. Lett.* **87** (16), 160601 (2001).
- [17] Y. Deng, T. M. Geroni and A. D. Sokal, *Phys. Rev. Lett.* **99** 110601 (2007).
- [18] S. Chandrasekharan, *PoS LATTICE2008*, 003 (2008).
- [19] U. Wolff, *Nucl. Phys. B* **810**, 491 (2009).
- [20] U. Wolff, *Nucl. Phys. B* **814** 549 (2009).
- [21] R. Horsley and U. Wolff, *Phys. Lett. B* **105**, 290 (1981).
- [22] V. Azcoiti, J.L. Cortes, G. Di Carlo, A.F. Grillo and A. Tarancon, *Z. Phys. C* **47**, 247 (1990).